Journal of Marine Research, 68, 523–539, 2010

Measuring lateral heat flux across a thermohaline front: A model and observational test

by Barry R. Ruddick[1,2], Neil S. Oakey[1,3] and Dave Hebert[3]

ABSTRACT

We develop and test a method to observationally estimate lateral intrusive heat flux across a front. The model combines that of Joyce (1977), in which lateral cross-frontal advection by intrusions creates vertical temperature gradients, and Osborn and Cox (1972) in which vertical mixing of those gradients creates thermal microstructure that is dissipated by molecular conduction of heat. Observations of thermal microstructure dissipation χ_T are then used to estimate the production by intrusions, and hence the lateral heat flux and diffusivity. This method does not depend on the precise mechanism(s) of mixing, or on the dynamical mechanisms driving the frontal intrusions. It relies on several assumptions: (1) lateral cross-frontal advection produces diapycnal temperature gradients that are mixed locally, (2) thermal variance is dissipated locally and not exported, (3) intrusion scales are larger than turbulence scales, and (4) isotropy of temperature microstructure is assumed in order to estimate χ_T.

The method is tested using microstructure observations in Meddy "Sharon," where the erosion rate and associated lateral heat flux are known from successive mesoscale hydrographic observations (Hebert *et al.,* 1990). An expression is developed for the production (lateral heat flux times lateral temperature gradient, expected to equal χ_T) in a front of steady shape that is eroding (detraining) at a steady rate; the production is proportional to the erosion speed and the square of the cross-frontal temperature contrast, both of which are well-known from observations. The qualitative structure and integrated value of the dissipation agree well with model assumptions and predictions: thermal variance produced by lateral intrusive heat flux is dissipated locally, dissipation in intrusive regions dominates total dissipation, and the total dissipation agrees with the observed erosion rate, all of which suggests that microstructure observations can be used to estimate intrusive heat flux. A direct comparison was made between lateral heat flux estimated from mesoscale Meddy structure plus the known rate of erosion, and lateral flux based on microscale temperature dissipation, with excellent agreement in the frontal zone and poorer agreement where lateral temperature gradient is too small to accurately measure.

1. Introduction

Thermohaline intrusions have been found at virtually all oceanic fronts, and have been associated with cross-frontal lateral fluxes of heat, salt and mass, and could also be

1. Department of Oceanography, Dalhousie University, Halifax, N.S., Canada
2. Corresponding author: ***email: barry.ruddick@dal.ca***
3. Fisheries and Oceans Canada, Bedford Institute of Oceanography, Dartmouth, N.S. Canada

associated with lateral fluxes of dynamical quantities such as momentum, angular momentum, and potential vorticity. Intrusions exhibiting thermohaline inversions coherent over very large lateral scales (hundreds to thousands of km) have been observed in the Arctic (Carmack *et al.,* 1998), and the equatorial Pacific (Richards, 1998). Both of these are associated with global-scale water masses, and the effects of these intrusions may have significant large-scale consequences. See Ruddick and Richards (2003) for a recent review of observational studies of oceanic intrusions.

Because intrusive cross-frontal heat fluxes $\overline{\tilde{u}\tilde{T}}$ (where $\tilde{u}$ is the cross-frontal velocity and $\tilde{T}$ the temperature pertubation) are associated with small cross-frontal velocities of O (1 mm s^{-1}), they are exceptionally difficult to measure directly. Covariance of temperature and velocity observations have been used to measure intrusive heat flux in a laboratory simulation (Ruddick *et al.,* 1999), but in the ocean much stronger internal wave and inertial motions of several cm/s mask the much lower intrusion velocities. In a landmark study of intrusions in the Antarctic Circumpolar Front south of New Zealand, Joyce *et al.* (1978) found a dominant intrusion scale, lateral coherence, and persistent cross-frontal slope, all suggestive of a dynamical cause. They applied Joyce's (1977) model, assuming a constant vertical diffusivity, to estimate a lateral diffusivity of approximately 30 $m^2\ s^{-1}$, resulting in an estimated heat flux comparable to that by baroclinic instability and eddying. The above mentioned Arctic and equatorial Pacific intrusions were estimated by the same method to carry even larger heat fluxes. In view of the potential importance of lateral intrusive fluxes in these and many other fronts and the near-impossibility of their direct field measurement, an improved observational method of estimating heat fluxes would be valuable. The absence of a field-tested theory of intrusions that predicts finite-amplitude fluxes makes this goal even more desirable.

a. Mixing of a Mediterranean Salt Lens ("Meddy")

Armi *et al.* (1988; 1989) describe the structure and evolution of Meddy "Sharon" over a two-year period in which hydrographic and velocity observations showed significant decay. Multiple surveys and the fact that the Meddy core was isolated from surface and topographic influences meant that several key rates and fluxes (horizontal intrusion velocity, lateral and vertical diffusivities) involved in the thermohaline intrusive process were accurately estimated. Several pieces of circumstantial evidence implicated thermohaline intrusions as the prime agent of lateral mixing. The Meddy core had radially uniform salinity and temperature, and was smoothly stratified and stable to double-diffusive processes, surrounded by thermohaline intrusions at its edge (Fig. 1). A qualitative association was noted between the location of high levels of thermal microstructure, thermohaline intrusions, and the thermohaline front at the edge of the core. This front also coincided approximately with the radius of maximum radial circulation $rv(r)$ (i.e., the radius at which the vorticity changed sign). Over the first year of observation (surveys 1–3), the core decreased in radius by 30 km, and the zone of intrusions moved inward with the salinity front.

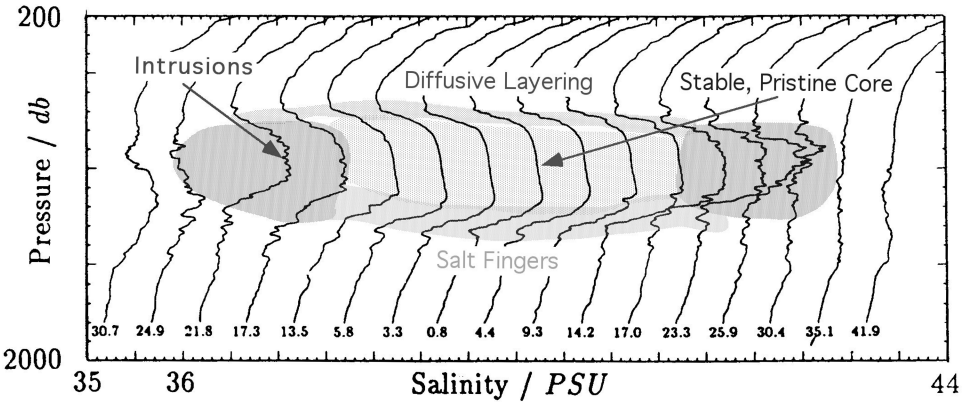

Figure 1. Waterfall plot of the salinity structure of Meddy "Sharon" as observed during the June 1985 survey. The salinity scale is correct for the leftmost trace; subsequent traces are offset by 0.5 PSU with the radius of each cast in km indicated at the bottom of the trace. The qualitative hydrographic structure and its stability to double-diffusive instabilities is indicated with gray shading.

Hebert (1988) interpreted the time evolution of thermohaline structure in the salt-finger stratified central "underbelly" of the Meddy in terms of vertical fluxes, finding diapycnal diffusivities consistent with those estimated by Kunze (1987), similar to diffusivities in C-SALT (Schmitt, 1981), and concluded that vertical salt finger fluxes alone would lead to a 20-year decay time. Hebert *et al.* (1990) diagnosed the radial evolution of the thermohaline structure to estimate a radial diffusivity of approximately 1–4 $m^2\ s^{-1}$, and estimated a frontal detrainment rate of 0.4 mm s^{-1}.

A number of investigators have examined Meddy "Sharon" observations with respect to intrusion scales (Ruddick and Hebert, 1988; Walsh and Ruddick, 1995; 2000; Mueller *et al.,* 2007; Smyth and Ruddick, 2010), density anomalies (Ruddick and Walsh, 1995), slopes relative to isopycnals (Ruddick, 1992; Kuz'mina and Rodionov; 1992; May and Kelley, 1997), and found the intrusive structure to be generally consistent with thermohaline intrusions driven by a combination of double-diffusion and turbulence, plus the possibility of baroclinic energy release.

The above findings suggested that Meddy "Sharon" was primarily eroded and mixed into the surrounding ocean by thermohaline intrusions. The repeated surveys and isolation from the surface allowed accurate estimates of net changes, fluxes and mechanisms, so that the front surrounding Meddy "Sharon" is a good model for other thermohaline fronts where it is more difficult to directly estimate the fluxes or observe the effects of mixing.

b. Goals of this study

The specific question addressed in this paper is: can the observed microstructure dissipation rates be related to the intrusion process and the mesoscale changes in the Meddy? We use the model of Joyce (1977) to link lateral heat flux to diapycnal mixing

(Section 2b), and the model of Osborn and Cox (1972) to link diapycnal mixing to thermal variance dissipation (Section 2a). The resulting relationship (Section 2c) allows lateral heat flux across fronts to be estimated from thermal microstructure, and does not depend on the precise mechanisms of mixing (fingers, double-diffusion, cabelling, turbulence or any combination) nor on the dynamical mechanisms (double-diffusion, McIntyre, or baroclinic instability, for example) driving the frontal intrusions. We then relate frontal erosion (detrainment) rate in the Meddy to the net horizontal production term for thermal variance. The combination results in an estimate of the volume-integrated thermal dissipation in the front (Section 2d), which compares well (qualitatively and quantitatively) with microstructure observations of thermal dissipation. A direct comparison of the production rate (radial temperature flux times radial temperature gradient) deduced from the observed temperature structure and erosion rate with microstructure dissipation validates the method.

2. The models

a. The Osborn-Cox (1972) model

Osborn and Cox (1972) developed the classical model for the quantitative interpretation of temperature microstructure observations. They began with conservation of temperature, T:

$$\frac{dT}{dt} + u_3\Gamma = \kappa_T \nabla^2 T, \tag{2.1}$$

where u_i indicates the i^{th} component of velocity and Γ is the adiabatic lapse rate, used in computing potential temperature. They partitioned into mean ($\tilde{}$) and turbulent ($'$) velocity and temperature, and obtained a conservation law for microscale thermal variance, $\widetilde{T'^2}$ (Gregg, 1987):

$$\frac{\partial \widetilde{T'^2}}{\partial t} + \frac{\partial}{\partial x_i}\left[\tilde{u}_i \widetilde{T'^2} + \widetilde{u_i T'^2} - \kappa_T \frac{\partial \widetilde{T'^2}}{\partial x_i}\right] + 2\,\widetilde{u_i' T'}\left[\frac{\partial \tilde{T}_i}{\partial x_i} + \tilde{\Gamma}\delta_{i3}\right] = -2\kappa_T \widetilde{\left[\frac{\partial T'}{\partial x_i}\right]^2}, \tag{2.2}$$

where repeated indices indicate summation from 1 to 3. The terms express, in order, (1) temporal rate of change, (2) divergence of mean, triple correlation, and diffusive flux, (3) horizontal and vertical production of thermal anomalies by stirring of fluid parcels in a thermal gradient, and (4) the dissipation of these anomalies by molecular heat conduction. For steady and homogeneous turbulence and vertical mean gradients a balance holds between (vertical) production, $P_v \equiv -2\widetilde{w'T'}\left[\frac{\partial \tilde{T}}{\partial z} + \tilde{\Gamma}\right]$, and dissipation $\chi_T \equiv 2\kappa_T[\widetilde{\nabla^2 T'}]$:

$$P_v = \chi_T. \tag{2.3}$$

With sufficient averaging, high-resolution temperature profiles can be used to estimate the diapycnal heat flux by turbulence, double-diffusion, and/or salt fingers (Ruddick *et al.,* 1997; St. Laurent and Schmitt, 1999), although the assumption of isotropy has been

questioned. When expressed in terms of a vertical eddy diffusivity for heat, (2.3) becomes the classical Osborn-Cox model:

$$\tilde{K}_{vT} = \frac{\tilde{\chi}_T}{2[\partial\tilde{T}/\partial z + \tilde{\Gamma}]^2}. \tag{2.4}$$

Note that the diffusivity is not necessarily constant nor specific to the mechanism causing the diapycnal mixing.

Gregg (1987) pointed out that in frontal regions, lateral intrusions (and therefore the lateral production terms in (2.2)) contribute the most to production of thermal variance, so the classical Osborn-Cox relationship (2.4) is not appropriate. Gargett (1978) noted that thermal variance produced at fronts is eventually dissipated at molecular scale. Winters and D'Asaro (1996) discuss the relation between stirring and (diffusive) mixing, showing how the diathermal diffusive heat flux is related to temperature variance dissipation, and outline a sorting technique that allows the dissipation term to be evaluated exactly for vertical temperature profiles in thermocline mixing. While they clearly show that all mixing leads to molecular dissipation, the lateral and vertical fluxes combine in a manner that is difficult to separate. It is thus difficult to use their approach to deduce lateral thermohaline fluxes.

b. The Joyce (1977) model

Joyce (1977) applied the concepts of Osborn and Cox to lateral intrusive mixing across a front. He defined three distinct scales: the frontal, or mesoscale ($\bar{}$), the intrusion scale ($\tilde{}$), and the microscale ($'$). He defined an averaging procedure such that the temperature was composed of the sum of contributions from the three scales:

$$T = \bar{T} + \tilde{T} + T'. \tag{2.5}$$

He then averaged the temperature variance equation on the intrusive and mesoscales to quantify the arguments of Stommel and Fedorov (1967): *lateral advection by intrusions produces thermohaline anomalies that are erased by diapycnal mixing.* The diapycnal mixing produces microscale anomalies that are then erased by molecular diffusion (Fig. 2).

Joyce showed that on the mesoscale (frontal scale), lateral production of thermal anomalies by intrusions balances vertical mixing of heat across the intrusions:

$$P_H \equiv -\overline{2\tilde{u}\tilde{T}}\,\frac{\partial\bar{T}}{\partial x} = \overline{\tilde{K}_{vT}\left(\frac{\partial\tilde{T}}{\partial z} + \tilde{\Gamma}\right)^2} \tag{2.6}$$

or, in terms of a lateral eddy diffusivity for heat, $\bar{K}_H = -\overline{\tilde{u}\tilde{T}}\Big/\dfrac{\partial\bar{T}}{\partial x}$

$$\bar{K}_{HT} = \overline{\tilde{K}_{VT}\left(\frac{\partial\tilde{T}}{\partial z} + \tilde{\Gamma}\right)^2}\Bigg/\left(\frac{\partial\bar{T}}{\partial x}\right)^2. \tag{2.7}$$

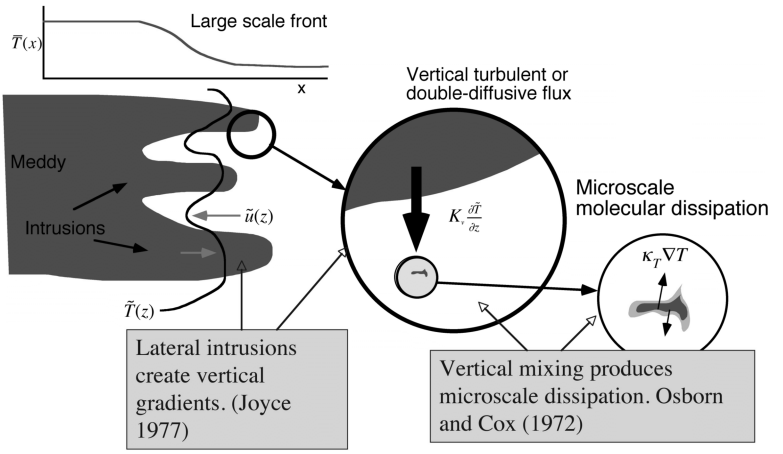

Figure 2. (After Joyce, 1977) Section in the cross-frontal plane (x,z) of an interleaving front aligned in the y-direction. The large-scale (∼3 km) frontal gradient in combination with fine-scale (tens of m. vertical scale) cross-frontal shears creates thermohaline intrusions. These intrusions are in turn acted upon by diapycnal mixing, which produces thermal variance that is dissipated at the molecular scale (∼cm). Measuring the microscale thermal dissipation allows the lateral heat flux in the x-direction to be estimated.

Joyce *et al.* (1978) assumed a constant value of $\tilde{K}_{VT}$ and used (2.7) to estimate a significant poleward intrusive heat flux across the Antarctic Circumpolar front. A disadvantage of that method is that a diapycnal diffusivity must be assumed, but this can be surmounted using Eq. (2.4).

c. The combined model ("Osborn-Cox works laterally")

Averaging (2.3) on the mesoscale and substituting into (2.6), we find that the lateral production of thermal variance P_H in (2.6) is balanced by vertical production, and hence in turn by microscale dissipation:

$$\boxed{P_H = \overline{P_V} = \overline{\chi_T}.} \tag{2.8}$$

In terms of a lateral flux,

$$\boxed{\overline{\tilde{u}\tilde{T}} = -\bar{\chi}_T \Big/ 2\left(\frac{\partial \bar{T}}{\partial x}\right).} \tag{2.9}$$

These relationships link the lateral intrusive heat flux and microscale dissipation. Note the similarity in form of (2.9) to the Osborn-Cox relationship (2.4), but for horizontal quantities. This is independent of the mechanisms driving the intrusions, whether double-

diffusion (Stern, 1967; McIntyre, 1970), or baroclinic driving (Kuz'mina and Rodionov, 1992; May and Kelley, 1997).

These results can be derived directly from the large-scale average of the thermal variance equation (2.2). Neglecting the temporal and divergence terms, but retaining both horizontal and vertical production terms:

$$2\overline{u_i'T'}\left[\frac{\partial \bar{T}}{\partial x_i} + \bar{\Gamma}\delta_{i3}\right] = \bar{\chi}_T. \tag{2.10}$$

The ratio of mean vertical production terms to horizontal is

$$\frac{\bar{K}_{VT}\left(\frac{\partial \bar{T}}{\partial z} + \bar{\Gamma}\right)^2}{\bar{K}_{HT}\left(\frac{\partial \bar{T}}{\partial x}\right)^2} \approx \frac{\bar{K}_{VT}\left(\frac{\partial \bar{T}}{\partial z} + \bar{\Gamma}\right)^2}{\overline{\left\{\tilde{K}_{VT}\left(\frac{\partial \tilde{T}}{\partial z} + \tilde{\Gamma}\right)^2\right\}}} \tag{2.11}$$

using (2.7). If the diapycnal eddy diffusivity is roughly independent of scale, so that $\tilde{K}_{VT} \approx \bar{K}_{VT}$, then (2.11) shows us that the ratio is small, and horizontal production terms dominate in fronts. If the vertical production term in (2.2) is neglected, we again obtain (2.8).

d. Detrainment across a front: An integral expression for χ_T

In this section we assume a front with a known and constant temperature difference across it. The front is assumed to erode at a constant rate c [m s^{-1}] with a shape that is constant. We first evaluate the integrated lateral production (Eq. 2.20) for a radially symmetric front (as for the Meddy), then derive a similar and even simpler result (Eq. 2.24) for a rectilinear front. We assume that the mesoscale temperature is of self-similar form $f(r + ct)$, with c the inward erosion speed (Fig. 3):

$$\bar{T}(r, t) = T_0 + \Delta T \cdot f(r + ct). \tag{2.12}$$

We define $\xi = r + ct$, and note that $f(0) = 1, f(\infty) = 0$. Then

$$\frac{\partial \bar{T}}{\partial t} = \Delta T c f', \tag{2.13}$$

a relationship that we will use below.

The conservation equation for mesoscale temperature is, in radial coordinates,

$$r\frac{\partial \bar{T}}{\partial t} = -\frac{\partial}{\partial r}(rF) \tag{2.14}$$

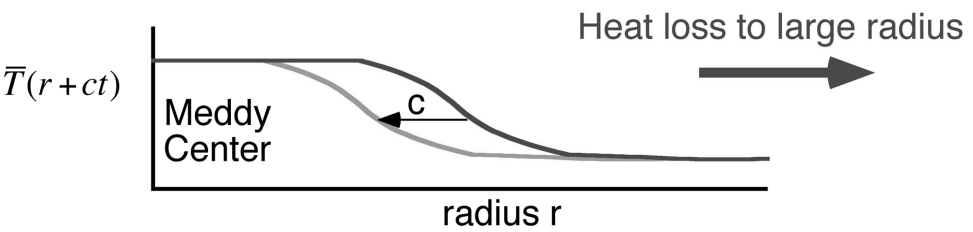

Figure 3. Sketch of a constant-form detraining front with temperature profile moving to the left at speed c.

where $F = \overline{\tilde{u}\tilde{T}}$ is the lateral intrusive heat flux. We take $F = 0$ at $r = 0$ (zero heat flux through the Meddy center), and integrate (2.14) to evaluate F at large radius r_0:

$$\begin{aligned}[rF(r)]_{r\to r_0} &= -\frac{\partial}{\partial t}\int_0^{r_0} r(\bar{T}(r,t) - T_0)dr \\ &= -c\Delta T\left\{\int_0^{r_0} \xi f'(\xi)d\xi\right\}.\end{aligned} \tag{2.15}$$

Since the quantity in {} brackets is constant, $F(r)$ decays inversely with radius at large radius. We will use (2.15) below.

We now estimate the radially integrated lateral intrusive production rate:

$$\mathbf{P}_H \equiv \int_0^\infty 2\pi r P_H dr = -\int_0^\infty 4\pi r F(r,t)\frac{\partial \bar{T}(r,t)}{\partial r}\,dr. \tag{2.16}$$

We next integrate by parts, using Eqs. (2.12) through (2.15)

$$\begin{aligned}-\mathbf{P}_H/4\pi &= -\int_0^\infty \bar{T}\frac{\partial}{\partial r}(rF)dr + [rF\bar{T}]_0^\infty \\ &= \int_0^\infty r\bar{T}\frac{\partial \bar{T}}{\partial t}\,dr + [rF\bar{T}]_0^\infty \\ &= \int_0^\infty r(T_0 + \Delta T f)\Delta T c f'\,dr + [rF]^{r=\infty}T_0 \\ &= T_0\Delta T c\int_0^\infty \xi f'\,d\xi + c\Delta T^2\int_0^\infty \xi f f'\,d\xi - T_0\Delta T c\int_0^\infty \xi f'\,d\xi.\end{aligned} \tag{2.17}$$

Since the first and third terms involving T_0, the temperature offset, cancel, we have

$$\boxed{\mathbf{P}_H = -4\pi c\Delta T^2 \int_0^\infty \xi f f' d\xi.} \tag{2.18}$$

This is an exact result for area-integrated dissipation (per unit depth) across any detraining front, in terms of the shape function of the front ($f(\xi)$), its erosion speed, c, and the temperature jump across it. The integral involving the shape function can be re-expressed as:

$$R_f \equiv -\int_0^\infty \xi f f' d\xi = +\frac{1}{2}\int_0^\infty f^2 d\xi, \tag{2.19}$$

which shows (since $f(0) = 1$) that the integral is related to the radius of the front. For a temperature shape function that decreases linearly from $f = 1$ at r_{min} to $f = 0$ at r_{max}, this integral becomes $R_f = r_{min} + (r_{max} - r_{min})/3$, which is about 25 km for the Meddy. Thus we have a simple expression for the integrated production, $\mathbf{P}_H$, which by (2.8) equals the integrated thermal dissipation:

$$\boxed{\mathbf{P}_H = \iint \chi dA = 2\pi R_f c\Delta T^2} \quad [\mathrm{C^2\ m^2\ s^{-1}}]. \tag{2.20}$$

We test this relationship in Section 3 against observations of thermal dissipation.

The analogous result for a rectilinear front is simpler to derive with a result that is completely independent of the details of the frontal profile. We assume a front of steady form moving to the left at speed c:

$$\bar{T}(x, t) = T_0 + \Delta T \cdot f(x + ct). \tag{2.21}$$

We define $\xi = x + ct$, and note that $f(0) = 1, f(\infty) = 0$. Then (2.13) holds as in the radial case. Conservation of mesoscale temperature is

$$\frac{\partial \bar{T}}{\partial t} = -\frac{\partial F}{\partial x} \tag{2.22}$$

where F is the cross-frontal intrusive heat flux. We take $F = 0$ at $x = 0$, and integrate (2.22) using (2.13) to obtain F:

$$\begin{aligned} F(x) &= -c\Delta T \int_0^x f'(x + ct)dx \\ &= -c\Delta T f(x + ct) + const. \\ &= c\Delta T(1 - f(x + ct)). \end{aligned} \tag{2.23}$$

This allows us to evaluate the net production *per unit length* alongfront:

$$\begin{aligned}
\mathbb{P}_{Net} &\equiv -2\int_0^\infty F(x,t)\,\frac{\partial \bar{T}}{\partial x}\,dx \\
&= -2c\Delta T^2\int_0^\infty (1-f(x+ct))\,\frac{\partial f(x+ct)}{\partial x}\,dx \\
&= -2c\Delta T^2\left[\int_0^\infty f'(\xi)d\xi - \int_0^\infty f(\xi)f'(\xi)d\xi\right], \\
&= -2c\Delta T^2\left[[f]_0^\infty - \tfrac{1}{2}\int_0^\infty (f^2)_\xi d\xi\right] \\
&= -2c\Delta T^2\left[f-\tfrac{1}{2}f^2\right]_0^\infty \\
&= +2c\Delta T^2
\end{aligned} \tag{2.24}$$

a result similar to 2.20 but completely independent of the shape of the front.

3. Comparison with observations

According to (2.8), the lateral production of thermal variance as estimated by (2.20) (or 2.24 for a linear front) should be equal to the thermal dissipation χ_T if the lateral Osborn-Cox relationship (2.10) holds and if lateral production dominates dominates large-scale vertical production as demonstrated in (2.11).

a. Lateral production

In order to estimate the radial production rate from mesoscale observations of Meddy "Sharon" we used radially binned and 10-m depth averaged temperature structure from the June 1985 CTD survey. This was interpolated to 0.5 km spacing using cubic spline, smoothed with a 3.5 km running mean, then a centered difference was taken to estimate the radial temperature gradient. The frontal erosion speed c is 36 km/1000 days = 0.42 mm s^{-1} based on the rate of change of the salinity front radius R_f in Figure 5 of Hebert *et al.* (1990). Use of (2.23) to evaluate the flux gives an estimated production rate of

$$P_H = c[T(0,z) - T(r_0,z)]\,\frac{\partial T}{\partial x}, \tag{3.1}$$

where the quantity in square brackets is the temperature contrast between the Meddy center ($r = 0$) and well outside ($r = r_0 = 53$ km). (Note that 2.23 and 2.24 are based on Cartesian rather than cylindrical coordinates and is an approximation to the flux that would

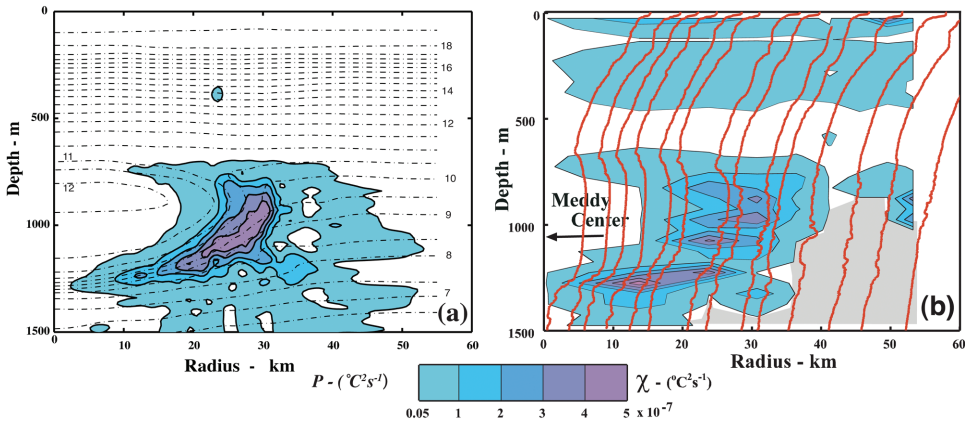

Figure 4. (a) Estimated rate of lateral production during the June 1985 Meddy survey based on Meddy temperature and assumed erosion speed. The temperature from CTD casts was averaged in unevenly spaced radius bins (Hebert *et al.,* 1990), cubic spline interpolated to 0.5 km radius intervals, and smoothed with 3.5 km running mean prior to being radially differentiated. Production was estimated as twice the lateral heat flux F (from 2.23) multiplied by smoothed radial temperature gradient. The lowest-value 0.05×10^{-7}°C^2 s^{-1} contour corresponds to EPSONDE instrumental noise level. The radially averaged, 3.5 km radially smoothed temperature is shown in black dash-dot contours with contour interval 0.5°C. (b) Microscale dissipation measured by EPSONDE, sorted into unevenly distributed radius bins and 50-m depth bins, plotted vs. depth and radius from center of Meddy. The gray shading at lower right indicates regions where no microstructure data were taken. Contour values and color bar match figure (a) for direct comparison. Temperature profiles (red) measured by CTD are plotted such that the trace position at 1500 m indicates the CTD cast radius.

be deduced from a more difficult analysis in radial coordinates.) Figure 4a shows the estimated lateral production rate (°C^2 s^{-1}) from the erosion speed and smoothed temperature, with (dot-dashed) contours of smoothed temperature superimposed so that the relationship between Meddy structure and required mixing can be clearly seen. The most intense production is predicted to be in the frontal zone of the Meddy, extending more below than above the Meddy "equator" at 1000-m depth. This will be compared with observed dissipation in Section 3b, using confidence intervals discussed in Section 3d.

b. Microscale thermal dissipation

As part of the June 1985 survey of Meddy "Sharon," 95 stations were taken using the tethered free-fall profiler EPSONDE (Oakey, 1988a), which sampled microscale temperature and shear, plus fine scale temperature and conductivity (Oakey, 1988b) while being allowed to free-fall at approximately 0.9 m/s to depths of about 1500 m. An overview of the thermal microstructure and how it relates to the Meddy hydrography is in Figure 12 of Armi *et al.* (1989). Thermal dissipation profiles were calculated as described in Oakey (1988b), and the profiles were averaged in unequal radius bins using an area-weighted

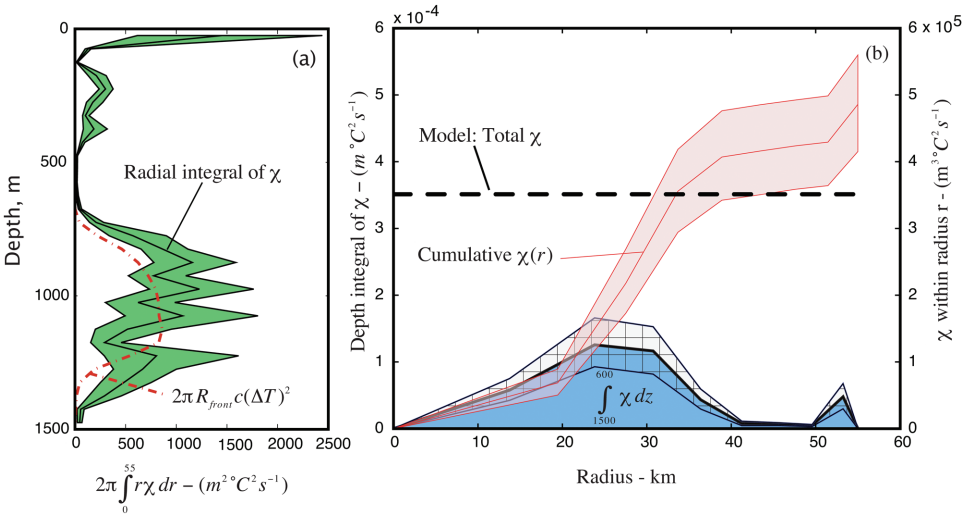

Figure 5. (a) Microscale thermal dissipation integrated radially within each depth bin (solid black trace), with statistical uncertainty estimated via bootstrap calculations described in Section 3d (green shading), and theoretical estimate (2.20) of lateral intrusive production of thermal variance (red dash-dot curve) calculated with parameters as described in the text. (b) Thermal dissipation integrated vertically between 600-m and 1500-m depth (blue-filled curve) with bootstrap-estimated uncertainty shown via cross-hatching; scale on left axis. Radially cumulative dissipation (solid red curve) and bootstrap-estimated uncertainty (light red shading); scale on right axis. The theoretical estimate of volume-integrated dissipation (2.20) is the horizontal dashed black line.

scheme to obtain the smoothed χ_T distribution contoured in Figure 4b. Note the excellent qualitative and quantitative agreement between χ_T and estimated production for depths greater than 600 m. The fact that frontal zone dissipation values are several times larger than in the core and outside of the Meddy confirms the estimate (2.11) that intrusive production is much larger than large-scale vertical production.

We estimate the frontal radius as $R_{front} = 25$ km at the time of the June 1985 survey (Figs. 3b and 5 of Hebert *et al.,* 1990). The temperature contrast $\Delta T(z)$ between the Meddy core and surrounding waters was estimated from 100-m averages of CTD profiles at Meddy Center and at large radius, from the June 1985 survey. These values were used in (2.20) for comparison with radial and vertical integrals of the observed dissipation.

Despite strong dissipation above and below the Meddy core, the intrusive zone between 20 and 30 km radius contributes most strongly to the volume integrated χ_T (Fig. 5b). There is a significant "burst" of dissipation near 900 m, 53 km radius (Fig. 4b) that contributes several percent to the cumulative dissipation, but this appears to be outside the Meddy and its frontal zone. Figure 4b agrees well with the estimated lateral production in Figure 4a for depths exceeding 500 m. The broad area of moderate dissipation above 500 m is associated with thermocline mixing with estimated diffusivity 3×10^{-5} m^2 s^{-1}, possibly enhanced due to salt finger stratification.

The agreement between estimated production (Figure 4a) and observed dissipation (Fig. 4b), and the quantitative agreement between χ_T and the vertical (Fig. 5a), radial (Fig. 5b), and fully integrated (Fig. 5b) profiles derived from (2.20), supports the models of Section 2 and suggests that a local balance exists between lateral production and dissipation.

c. Lateral heat flux and diffusivity

Figure 6 shows the radial temperature gradient (solid curve, negative values) and the lateral heat flux estimated from (3.1) (dash-dot curve), and the microstructure-based estimate (Eq. 2.9) of lateral heat flux, with all quantities averaged over 600 m–1300 m depth. Bulk and microstructure-based flux estimates agree well within the frontal zone, where dissipation greatly exceeds background and noise levels, and where radial temperature gradient is large enough to be well-estimated. Disagreement is apparent outside of the frontal zone, where dT/dr is small and highly uncertain. We have therefore not attempted to compute or show estimated uncertainties in Figure 6. The ratio of flux to gradient at 25 km radius is consistent with a lateral eddy diffusivity of 3 $m^2\ s^{-1}$. Notice, however, that pointwise estimates of lateral diffusivity by this method are extremely noisy due to division by small gradients (squared) near the edges of the front. Hebert *et al.* (1990) estimated the lateral salt diffusivity as either 1–2 or 2–4 $m^2\ s^{-1}$, depending on the type of bulk estimate used.

An examination of (2.23) (or 2.15) tells us that the heat (and salt) flux must increase from zero at $r = 0$ to a maximum at large r, as shown in Figure 6. This leads to a paradox: How can the flux be large at large radius where intrusions are demonstrably weak? Hebert *et al.*(1990) found the salinity and heat content of the Meddy decreased during the period of observations, so this heat and salt must be transported away from the Meddy—a flux that extends beyond the intrusive zone. We suggest that the intrusive mixing altered the salinity, temperature, velocity and potential vorticity profiles of the Meddy and that these alterations acted as a catalyst for surrounding mesoscale strain and shear motions to remove material from the outer range of the Meddy front, a process that would be consistent with our observations. Some Meddies have been observed to fragment upon collision with other mesoscale features or seamounts (Richardson *et al.,* 2000), and others may "shed" intrusive zones when interacting with large-scale strains (Brickman and Ruddick, 1990), but we found that intrusions surrounding Meddy "Sharon" appear to be dissipated locally. The far-field transport and mixing into background of the lost salt and heat content should result in some form of "excess" dissipation—the signal of final blending of the Meddy's "salty trail." The region of high thermal dissipation and apparent thermohaline intrusions at radius of 55 km and depth of 1000 m in Figure 4 could be part of this "trail." The heat and salt transport at large radius may be caused by lateral stirring by mesoscale eddies.

d. Confidence intervals for integrated χ_T

In order to provide an estimate of the uncertainty in the integrated thermal dissipation, the 95% confidence limits were determined by the bootstrap method. Standard processing

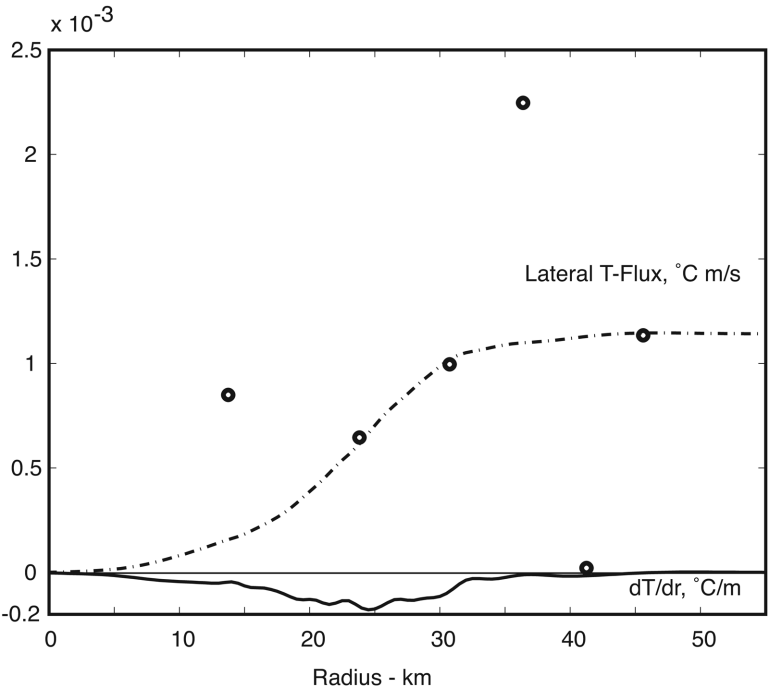

Figure 6. Radially smoothed temperature gradient (solid curve), lateral heat flux (dash-dot curve) estimated from (3.1) using smoothed temperature structure (described and shown in Figure 4), and lateral heat flux estimated using (2.9) from thermal dissipation and temperature gradient (circles). Negative heat flux estimates of -0.0015 and -0.044°C ms^{-1} at r = 49.5 and 53.25 km respectively are associated with small positive *dT/dr* and are not shown. Temperature, its radial gradient, and thermal dissipation were averaged over 700–1300-m depth range.

techniques (Oakey, 1988a; 1982) were used to generate estimates of χ_T for individual segments (approximately every 8 meters vertically) for each profile. These segments were edited and bad data removed. If the signal level was less than the noise level, χ_T was assigned a value of 0. All of the segments were sorted into radial and vertical bins as described earlier. For some of the bins used in the integration (those at the outer lower edge of the Meddy—see Fig. 4b), that had no data or one χ_T estimate, we included an estimate of χ_T based on adjacent mean values inward and above that bin. If no data existed, we also included zero as an estimate of χ_T. Thus, we are providing estimates of the range of χ_T that could be found in that location. For the bootstrap calculation, the mean χ_T in each bin was determined using the method of Efron and Gong (1983) and those mean values were integrated vertically and horizontally. This procedure was repeated 1000 times and the corresponding 95% confidence intervals are shown in figure 5 as shaded or hatched regions. The statistical uncertainty in radially or vertically integrated χ_T profiles is approximately $\pm 30\%$, and reduces to $\pm 15\%$ for the cumulative total.

Oakey (1982) discusses a number of other factors leading to uncertainty in χ_T, including systematic errors arising from probe calibration, electronics calibration, and probe frequency response (12% rms), random errors in determining sensor velocity and noise subtraction (15% rms). The statistical uncertainties in integrated χ_T in Figure 5 are considered to include the random error above, but exclude systematic errors. Additional uncertainty results from the aforementioned assumption of statistical isotropy.

4. Summary and discussion

We developed a model that combines the intrusion model of Joyce (1977) with the diapycnal mixing model of Osborn and Cox (1972), allowing estimation of lateral intrusive heat flux from microscale thermal dissipation. The result is simple: lateral intrusive production leads to vertical production that is dissipated locally. The key assumptions are that lateral intrusive production dominates over large scale vertical/diapycnal production (Eq. 2.11), and that production and dissipation balance locally within the intrusive region. We test the integrated balance using a simple model of a detraining front that expresses the lateral thermal production in terms of the detrainment speed and cross-frontal temperature contrast. The comparison with observed microscale thermal dissipation yielded the following conclusions:

1. Regions of intense thermal dissipation coincide with the diffusive layering and finger layering zones above and below the Meddy core, and with the intrusive zone surrounding the core. This was shown qualitatively in Armi *et al.* (1988), and more quantitatively in Figure 4.
2. The observed thermal dissipation in the intrusive zone (Fig. 4b) quantitatively and qualitatively matches the estimated lateral production at depths below 600 m (Fig. 4a).
3. The intrusive zone is the greatest contributor to the volume-integrated dissipation (Fig. 5).
4. The volume integral of thermal dissipation is consistent with the net production estimated from observed bulk rate of Meddy erosion, which supports a local production/dissipation balance.
5. Eqs. 2.8 and 2.9 allow lateral heat flux and diffusivity to be estimated from microstructure observations in a manner similar to the Osborn-Cox method, although small and noisy gradients appearing in the denominator of those equations demand careful attention (Fig. 6).

The concept described here is not new: Gargett (1978) noted that thermal variance production by lateral heat flux is dissipated at molecular scale, and Gregg (1987) pointed out the potential contribution of lateral processes in frontal zones. Gregg (1987) suggests that the second term of Eq. 2.2 (divergence of the triple correlation) may be significant in intrusive regions, but the close spatial match between lateral production and microscale dissipation suggests otherwise. Garrett (2001) discusses the triple decomposition in the Joyce model, noting the possibility of multiple pathways for thermal variance. We have

concluded that the pathway in #4 above dominates in frontal zones (Eq. 2.11), and dominates the Meddy-scale average.

Eqs. (2.8) and (2.24) for a one-dimensional front can also be applied in a completely different context: to relate the rate of entrainment and associated irreversible mixing to the depth-integrated thermal dissipation near the mixed layer base. This would allow observations of χ_T to be used to directly measure the entrainment rate. It should be feasible to test this application in a relatively simple laboratory experiment in which grid-stirred turbulence causes mixed layer deepening in temperature stratification. It may be feasible to directly measure microscale temperature gradients using optical or acoustic techniques, or with probes designed to measure microscale conductivity gradient. We look forward to hearing of such experiments.

Acknowledgments. We thank the Canadian Natural Sciences and Engineering Research Council and Fisheries and Oceans Canada for support, and gratefully acknowledge our colleagues from the Meddy "Sharon" experiment. We wish to thank Eric D'Asaro for useful discussions about the WD concepts, and also to apologize for our lack of active collaboration to date in application of WD concepts to this data set.

REFERENCES

Armi, L., D. Hebert, N. Oakey, J. Price, P. Richardson, T. Rossby and B. Ruddick. 1988. The movements and decay of Mediterranean Salt Lens. Nature, *333,* 649–651.

—— 1989. Two years in the life of a Mediterranean salt lens. J. Phys. Oceanogr., *19,* 354–370.

Brickman, D. and B. Ruddick. 1990. The behavior and stability of a lens in a strain field. J. Geophys. Res., *95,* 9657–9670.

Carmack, E., K. Agaard, J. Swift, R. Perkin, F. McLaughlin, R. Macdonald and P. Jones. 1998. Thermohaline transitions, *in* Physical Processes in Lakes and Oceans, J. Imberger, ed., Coastal Estuar. Studies, *54,* 179–186.

Efron, B. and N. Gong. 1983. A leisurely look at the Bootstrap, the Jacknife, and Cross-Validation, The American Statistician, *37,* 36–48.

Gargett, A. E. 1978. Microstructure and fine structure in an upper ocean frontal regime. J. Geophys. Res., *83,* 5123–5134.

Garrett, C. 2001. Stirring and mixing: What are the rate-controlling processes? Proceedings of the Twelfth ʻAha Huliko'a Hawaiian Winter Workshop, 1–8.

Gregg, M. C. 1987. Diapycnal mixing in the thermocline: A review. J. Geophys. Res., *92(C5),* 5249–5286.

—— 1975. Microstructure and intrusions in the California Current. J. Phys. Oceanogr., *5,* 253–278.

Hebert, D. 1988. Estimates of salt finger fluxes. Deep-Sea Res., *35,* 1887–1901.

Hebert, D., N. Oakey and B. R. Ruddick. 1990. Evolution of a Mediterranean Salt Lens: Scalar Properties. J. Phys. Oceanogr., *20,* 1468–1483.

Joyce, T. M. 1977. A note on the lateral mixing of water masses. J. Phys. Oceanogr., *7,* 626–629.

Joyce, T. M., W. Zenk and J. M. Toole. 1978. The anatomy of the Antarctic polar front in the Drake Passage. J. Geophys. Res., *83,* 6093–6113.

Kunze, E. 1987. Limits on growing, finite-length salt fingers: a Richardson number constraint. J. Mar. Res., *45,* 533–556.

Kuz'mina, N. P. and V. B. Rodionov. 1992. Influence of baroclinicity on formation of thermohaline intrusions in ocean frontal zones. Izv. Atmos. Oceanic Phys., *28 (10–11),* 804–810.

May, B. D. and D. E. Kelley. 1997. Effect of baroclinicity on double diffusive interleaving. J. Phys. Oceanogr., *27,* 1997–2008.

McIntyre, M. 1970. Diffusive destabilization of the baroclinic circular vortex. Geophys. Fluid Dyn., *1,* 19–57.

Mueller, R. D., W. D. Smyth and B. R. Ruddick. 2007. Shear and convective turbulence in a model of thermohaline intrusions. J. Phys. Oceanogr., *37,* 2534–2549.

Oakey, N. S. 1982. Determination of the rate of dissipation of turbulent energy from simultaneous temperature and velocity shear microstructure measurements. J. Phys. Oceanogr., *12,* 256–271.

—— 1988a. Epsonde: An instrument to measure turbulence in the deep ocean. IEEE J. Oceanic Eng., *13,* 124–128.

—— 1988b. Estimates of mixing inferred from temperature and velocity microstructure, *in* Small-scale Turbulence and Mixing in the Ocean, J. Nihoul and B. Jamart, eds., Elsevier Oceanography Series, NY, 239–248.

Osborne, T. R. and C. S. Cox. 1972. Oceanic fine structure. Geophys. Fluid Dyn., *3,* 321–345.

Richards, K. J. 1998. Interleaving at the equator, *in* Ocean Modelling and Parameterization, E. P. Chassignet and J. Verron, eds., Proceedings of NATO ASI Series C, *516,* Kluwer., 235–252.

Richardson, P. L., A. S. Bower and W. Zenk. 2000. A census of Meddies tracked by floats. Prog. Oceanogr. *45,* 209–250.

Ruddick, B. R. 1992. Intrusive mixing in a Mediterranean salt lens—intrusion slopes and dynamical mechanisms. J. Phys. Oceanogr., *22,* 1274–1285.

Ruddick, B. and D. Hebert. 1988. The mixing of Meddy "Sharon" *in* Small-Scale Turbulence and Mixing in the Ocean, J. Nihoul and B. Jamart, eds., Elsevier Oceanography Series, *46,* Elsevier, NY, 249–262.

Ruddick, B. R., O. M. Phillips and J. S. Turner. 1999. A laboratory and quantitative model of finite-amplitude intrusions. Dyn. Atmos. Oceans, *30,* 71–99.

Ruddick, B. and K. Richards. 2003. Oceanic thermohaline intrusions: observations. Prog. Oceanogr., *56 (3–4),* 499–527.

Ruddick, B. R. and D. Walsh. 1995. Observations of the density perturbations which drive thermohaline intrusions. Proceedings of the Chapman Conference on Double Diffusion, A. Brandt and J. Fernando, eds., Geophysical Monograph *94,* 329–334 (AGU Press).

Ruddick, B. R., D. Walsh and N. Oakey. 1997. Variations in apparent mixing efficiency in the North Atlantic central waters. J. Phys. Oceanogr. *27,* 2589–2605.

Schmitt, R. 1981. Form of the temperature-salinity relationship in the central water: Evidence for double-diffusive mixing. J. Phys. Oceanogr., *11,* 1015–1026.

Smyth, W. D. and B. R. Ruddick. 2010. Effects of ambient turbulence on interleaving at a baroclinic front. J. Phys. Oceanogr. *40,* 685–712.

St. Laurent, L. and R. Schmitt. 1999. The contribution of salt fingers to vertical mixing in the North Atlantic Tracer Release Experiment. J. Phys. Oceanogr., *29,* 1404–1424.

Stern, M. E. 1967. Lateral mixing of water masses. Deep-Sea Res., *14,* 747–753.

Stommel, H. and N. K. Fedorov. 1967. Small scale structure in temperature and salinity near Timor and Mindinao. Tellus, *19,* 306–325.

Walsh, D. and B. R. Ruddick. 1995. Double-diffusive interleaving: the influence of non-constant diffusivities. J. Phys. Oceanogr., *25 (3),* 348–358.

—— 2000. Double-diffusive interleaving in the presence of turbulence—The effect of a nonconstant flux ratio. J. Phys. Oceanogr., *30,* 2231–2245.

Winters, K. B. and E. A. D'Asaro. 1996. Diascalar flux and the rate of fluid mixing. J. Fluid Mech. *317,* 179–193.

Received: *5 March, 2010;* revised: *20 December, 2010.*